other arboviruses tested (Chandipura, Dengue 1–4 serotypes and Japanese encephalitis).

Comparison of clinical features between CHIKV-positive and CHIKV-negative patients demonstrated arthralgia, myalgia and headache to be significantly associated with CHIKV confirmed cases (chi-square test, $P < 0.05$; Table 3). No correlation between POD and CHIKV titre was observed (Mann–Whitney U test, $P > 0.05$; Pearson correlation coefficient 0.080; $P = 0.276$). Similar results have been reported by Ray et al.[9] during a multi-centric study carried out in India to confirm CHIKV infection in patients using virological and serology based assays. It was also confirmed in the present study that CHIKV-specific IgM antibodies could be detected from 2 POD, though the percentage was low.

Reddy et al.[10] evaluated the sensitivity of different assays for definitive diagnosis of CHIKV in a small number of clinical samples ($n = 70$, 2–5 POD). In the present study, we used more clinical samples ($n = 180$) with different PODs (2–15 POD) from various geographical areas of India. Although we used samples from various PODs, the sensitivity and specificity of CHIK detection methods described in the present study are higher than those reported earlier[10]. qPCR has been found to be more sensitive than nested PCR during early PODs (1–3 days), and the IgM ELISA kit was found to be more effective to detect the presence of CHIK during late POD ($8 \leq$ days). The data from the present study as well as the earlier study[10] indicate that the application of both IgM ELISA and RT-PCR-based assays will be ideal for definitive diagnosis of CHIK during outbreaks.

1. Sudeep, A. B. and Parashar, D., Chikungunya: an overview. J. Biosci., 2008, 33, 443–449.
2. Hasebe, F. et al., Combined detection and genotyping of Chikungunya virus by specific reverse transcription-polymerase chain reaction. J. Med. Virol., 2002, 67, 370–374.
3. Pfeffer, M., Lisssen, B., Parker, M. D. and Kenney, R. M., Specific detection of Chikungunya virus using a RT-PCR/nested PCR combination. J. Vet. Med., 2002, 49, 49–54.
4. Pastorino, B., Bessaud, M., Grandadam, M., Murri, S., Tolou, H. J. and Peyrefitte, C. N., Development of a TaqMan RT-PCR assay without RNA extraction step for the detection and quantification of African Chikungunya viruses. J. Virol. Methods, 2005, 124, 65–71.
5. Parida, M. M., Rapid and real-time detection technologies for emerging viruses of biomedical importance. J. Biosci., 2008, 33, 617–628.
6. Shukla, J., Khan, M., Tiwari, M., Sannarangaiah, S., Sharma, S., Rao, P. V. and Parida, M., Development and evaluation of antigen capture ELISA for early clinical diagnosis of Chikungunya. Diagn. Microbiol. Infect. Dis., 2009, 65, 142–149.
7. Parashar, D., Paingankar, M. S., Kumar, S., Gokhale, M. D., Sudeep, A. B., Shinde, S. B. and Arankalle, V. A., Administration of E2 and NS1 siRNAs inhibits Chikungunya virus replication in vitro and protects mice infected with the virus. PLoS Negl. Trop. Dis., 2013, 7(9), e2405.
8. Hanley, J. A. and McNeil, B. J., A method of comparing the areas under receiver operating characteristic curves derived from the same cases. Radiology, 1983, 148, 839–843.
9. Ray, P. et al., Chikungunya infection in India: results of a prospective hospital based multi-centric study. PLoS One, 2012, 7(2), e30025.
10. Reddy, V., Ravi, V., Desai, A., Parida, M. M., Powers, A. M. and Johnson, B. W., Utility of IgM ELISA, TaqMan real-time PCR, reverse transcription PCR, and RT-LAMP assay for the diagnosis of Chikungunya fever. J. Med. Virol., 2012, 84, 1771–1778.

Estimation of monthly average sunshine duration over China based on cloud fraction from MODIS satellite data

Yongjian He[1,2], Xinfa Qiu[1,2,*], Yun Cao[1,2] and Yan Zeng[3]

[1]Key Laboratory of Meteorological Disaster of Ministry of Education, No. 219, Ningliu Road, Nanjing, Jiangsu, China
[2]School of Geography and Remote Sensing, Nanjing University of Information Science and Technology, No. 219, Ningliu Road, Nanjing, Jiangsu, China
[3]Jiangsu Research Institute of Meteorological Science, No. 2, Beijige, Nanjing, Jiangsu, China

The sunshine duration (SSD) model described herein combines meteorological observation data from an extensive network of weather stations, MODIS satellite cloud cover data, and a high-resolution digital elevation model to produce high-resolution SSD maps of China. The model yielded low difference between the measured and estimated values at 672 standard weather stations. The mean absolute bias error (MABE) of the monthly mean daily SSD for 2001–2003 was 0.15–0.26 h and the relative bias error (RABE) was 2.34–4.64%. To further validate the model, the observation data from the intensive weather stations (with high spatial resolution) in Jiangsu and Qinghai not used in the calculations, were used for comparison with the estimated values. The annual mean MABE values in Jiangsu and Qinghai during 2001–2003 were less than 0.5 h, and the annual mean RABE values below 5%. Thus, one can conclude that the SSD model is reliable and stable. The spatial distribution of the SSD was also examined, which indicated that the

*For correspondence. (e-mail: xfqiu135@nuist.edu.cn)

macroscopic distribution of SSD in China determined using MODIS satellite data was more objective and more detailed than the distribution by interpolation of weather station observations of SSD.

SUNSHINE duration (SSD), defined as the time during which direct solar radiation exceeds a certain threshold (typically 120 W/m^2)[1], is among the most important and widely used parameters in climate monitoring. It is important for various sectors, including tourism, public health, agriculture[2], vegetation modelling[3] and solar energy. SSD is also used in ecosystem, hydrological and biophysical modelling[4] and is a good estimator of global radiation[5–9], rendering it useful for quality control in global radiation data measurements[10]. Thus, research on SSD is important for weather services and in estimating solar energy.

SSD is a standard parameter in meteorological stations, and its measurement is specified by the World Meteorological Organization (WMO). The possibility of SSD mapping through station observations is limited as result of the heterogeneous station density and sporadic station network in many regions. In addition, station observations are point measurements with a limited scope over a larger region[11]. Traditionally, three main approaches have been utilized to derive SSD: the empirical equation method, the analytical method and the graphical method. The first method primarily uses meteorological data from a given number of weather stations in a research area and establishes a regional empirical equation for SSD with respect to the elevation, latitude and longitude[12,13]. This method is easy to understand and convenient, but neglects the effect of terrain shading because the number of weather stations is limited and the stations are always located at flat, open sites (or on the top of mountains).

An analytical method was proposed to calculate SSD for some idealized terrains using the formula for sunrise and sunset hour angle[14,15]. Considering the effect of the terrain, the graphical method combines the shaded plot of the measured sites and traces of the Sun's movement to determine SSD in the shaded location. For calculations, a theodolite must be used to measure the shaded map of the individual sites, which requires significant effort and is time-consuming. Therefore, given the limitations of the terrain data and calculation methods, the aforementioned methods are only used for single, infinite and inclined planes. With the development of space technology, especially the application of Geographical Information System (GIS), grid maps of the interpolated SSD station measurements can be produced. Dolinar[16] used Kriging to generate SSD maps of Slovenia. Hogewind and Bissolli[17] described several interpolation methods for constructing operational climate maps for Europe and the Middle East. These products extended the scope of SSD station data, but the uncertainty in the interpolation increases significantly in areas with low station density; also interpolation must account for the influence of topographic features. Moreover, SSD itself is highly variable as it depends on cloud cover. Given the ability of space-based instruments to detect clouds and the correlation between SSD and cloud cover, satellite data can be used to estimate SSD.

Based on previous research, this study aims to establish a model in which SSD is computed using digital elevation model (DEM) and satellite data, considering the influence of the terrain and cloud cover.

The data used in this study include the following: (1) meteorological observation data – the monthly mean observed value for the total cloud cover, low cloud cover, sunshine percentage and SSD at 672 standard Chinese weather stations from 2001 to 2003, and the monthly mean SSD at intensive weather stations (59 in Jiangsu Province and 15 in Qinghai Province). The observation data at the standard weather stations from 2001 to 2003 were used for the development of the model, and observation data at the intensive weather stations were applied for model validation; (2) remote sensing data – the monthly mean total cloud cover in China from 2001 to 2003 with a spatial resolution of 5 km × 5 km as obtained from the TERRA/MODIS (MOD06) cloud product of the total daily cloud cover using a geometric correction procedure, an image mosaic and by averaging the image superposition of the total daily cloud cover for each month; (3) basic geographic data – DEM data with a spatial resolution of 1 km × 1 km for China and the basic geographic information for the standard and intensive weather stations. Figure 1 provides the distribution of standard and intensive weather stations throughout China.
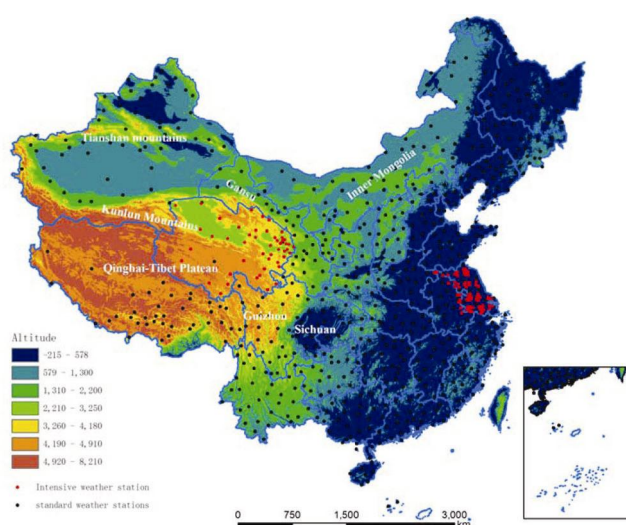
Figure 1. Distribution of standard and intensive weather stations throughout China and other places used in the study.

The observed sunshine percentage data from the weather stations are calculated as the ratio between SSD and the astronomical maximum PSD (possible sunshine duration) and range between 0 and 100 (as a percentage). The astronomical maximum PSD is defined as the maximum possible sunshine duration without considering atmospheric effects and terrain shading.

The total and low cloud cover recorded at the weather stations range from 0 to 10, where 0 corresponds to a clear sky with no clouds and 10 indicates a sky that is completely covered by clouds. The MODIS cloud product ranges between 0 and 1, where 0 indicates a clear sky and 1 indicates a sky that is completely obscured by clouds. For the sake of comparison, both weather station and MODIS cloud cover are given in percentage (i.e. the cloud cover in the sky was standardized for expression as a percentage corresponding to the sunshine percentage).

Studies have indicated that SSD at any point in the actual rugged terrain on a given day is the product of PSD in the rugged terrain and sunshine percentage[18]. The actual SSD in a rugged terrain ($L_{\alpha\beta}$) can be calculated as follows

$$L_{\alpha\beta} = L_{0\alpha\beta} \cdot SR, \tag{1}$$

where $L_{0\alpha\beta}$ is the PSD in the rugged terrain and SR the sunshine percentage. In this study, $L_{0\alpha\beta}$ is the geographical PSD which considers terrain shading but not the atmospheric effect and can be obtained from the distributed model of PSD in the rugged terrain[19]. The model uses the DEM data as input only and outputs the image data for the monthly PSD. Therefore, spatial analysis of the sunshine percentage is the key in SSD mapping.

Cloud cover is the main factor affecting the variability of the sunshine percentage[20]. Analysing monthly averages, we can assume that a negative linear relationship exists between these two values: the sunshine percentage decreases as the cloud cover increases, or the sunshine percentage increases as the cloud cover decreases. At present, the cloud cover is obtained from satellite retrievals or weather observations. Compared with observation data, the remote sensing cloud cover data have the advantages of broad coverage and a macroscopic spatial continuum, which can overcome the deficiencies in the observation data. Therefore, the remote sensing cloud cover data were introduced into the sunshine percentage model to account for the effect of the total and low cloud cover.

$$SR_g = a + b \cdot CL_g + c \cdot low_g, \tag{2}$$

$$SR = Interpolate(a) + interpolate(b) \cdot CL \\ + interpolate(c) \cdot low, \tag{3}$$

SR_g, CL_g and low_g are the sunshine percentage, total cloud cover and low cloud cover observed at weather stations respectively. The terms a, b and c are regression coefficients, CL, low and SR indicate the image data for total cloud cover, low cloud cover and the sunshine percentage respectively and interpolate(a) represents the interpolation result of the element a. The inverse distance weighted (IDW) interpolation method[21] was adopted in this study.

Research[22] has demonstrated that the satellite-retrieved cloud cover deviates from that observed at weather stations, and the satellite cloud cover data must be corrected prior to use. Therefore, the variable CL in eq. (3) represents the image data of the MODIS cloud cover after correction using the ratio correction method[23] as follows

$$R_{CL}^i = Interpolate\left(\frac{CL^p}{CL_g}\right), \tag{4}$$

$$CL = \frac{CL_S}{R_{CL}^i}, \tag{5}$$

where CL^p is the satellite-retrieved total cloud cover at the point corresponding to the weather station location, CL_g the total cloud cover observed at the weather station, R_{CL}^i indicates the interpolated image data for the ratio between CL^p and CL_g, and CL_S indicates the image data for the total cloud cover retrieved from the satellite.

Based on the ratio correction method, the image data for the low cloud cover and the variable low in eq. (3), the following formulae were derived

$$R^i = Interpolate\left(\frac{low_g}{CL_g}\right), \tag{6}$$

$$Low = CL \cdot R^i, \tag{7}$$

where low_g is the low cloud cover observed at the weather stations and R^i represents the interpolated image data for the ratio between the low and total cloud cover observed at the weather stations. Figure 2 provides a flow chart for calculating SSD.

The images of monthly mean sunshine percentage were derived using the observed total cloud cover, the low cloud cover and sunshine percentage observed at 672 standard weather stations during 2001, and the remote sensing data of the MODIS cloud cover from 2001. The interpolated SSD station measurements were utilized directly to obtain the images of the monthly mean sunshine percentage at the weather stations. After superimposing and averaging, the annual mean sunshine percentage images were obtained from the model estimation (Figure 3 a) and weather stations (Figure 3 b). A comparison of Figure 3 a and b indicates that the distribution patterns in sunshine percentage in China are generally consistent. The high- and low-value areas coincide in the

two plots with numerically similar values. The high-value areas are located in western Inner Mongolia and the southwestern Qinghai–Tibet Plateau, where the sunshine percentage reaches 80. The low-value areas are located in the Sichuan–Guizhou region, where the sunshine percentage is below 30. However, the differences between these two figures are significant in the areas with sparsely distributed stations. Figure 3 *a* provides greater detail in the Tianshan mountainous region, the western margin of the Qinghai–Tibet Plateau and the northern area of the Kunlun Mountains than Figure 3 *b*, which demonstrates the advantage of introducing remote sensing data into the models.

The image of the monthly mean PSD for each month in China was derived using DEM data from China with a 1 km × 1 km resolution. This image was combined with that of the monthly mean sunshine percentage to produce the image of the monthly mean SSD according to eq. (1). As clearly depicted in Figure 4, the macroscopic distribution of the annual mean total daily SSD in China in 2001 is greater in the north and west than in the south and east, which is due to the combined effect of the climate, cloud fraction, atmospheric transparency and geographic factors. As an average, the annual mean total daily SSD in China in 2001 is 6.5 h; the lowest SSD is in the Sichuan Basin, where the annual mean total daily SSD is 2–3 h; Gansu and the Inner Mongolia Plateau region have the highest SSD values, with annual mean total values of approximately 8–9 h. The influence of the regional factors on SSD is particularly evident in the mountainous areas with rugged terrain. It is a more objective and detailed mapping of SSD in China using a SSD model that considers the terrain and sky factors, especially in mountainous, plateau or desert regions with fewer weather stations.

To verify the accuracy of the SSD model, the SSD values extracted from the images of the monthly mean SSD according to latitude and longitude of the standard weather stations, were compared with the observational data of SSD at a standard weather station. Table 1 lists the difference between model and observed values of SSD. As presented in Table 1 in 2001, the mean absolute bias error (MABE) of the monthly mean total daily SSD is 0.15–0.26 h, the relatively bias error (RABE) is 2.45–4.43%, the annual mean of MABE is 0.19 h, and the annual mean RABE is 3.22%. These results indicate that the SSD model is relatively accurate. We also calculated the difference between model and observed values of SSD of 2002 and 2003. The annual mean of MABEs in 2002 and 2003 are 0.19 h, and the annual mean of RABEs are 3.21% and 3.26% respectively, values similar to the statistical simulation errors for 2001. Accordingly, the SSD model has a strong modelling capability with respect to temporal dimensions. The SSD data from the intensive stations in Jiangsu and Qinghai for 2001–2003, which did not take part in the model calculation, were used to verify the respective spatial dimensions of the modelling capability. As indicated in Table 1, the annual mean of MABE in Jiangsu for 2001–2003 is 0.25 h, and the annual mean of RABE is approximately 4.5%. In Qinghai, the annual
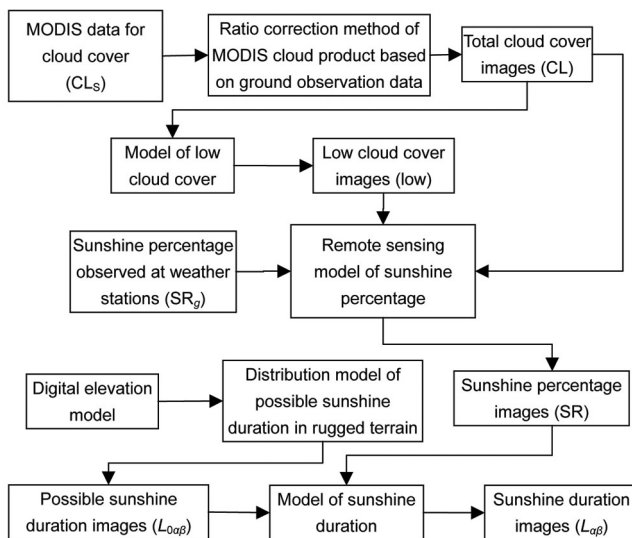

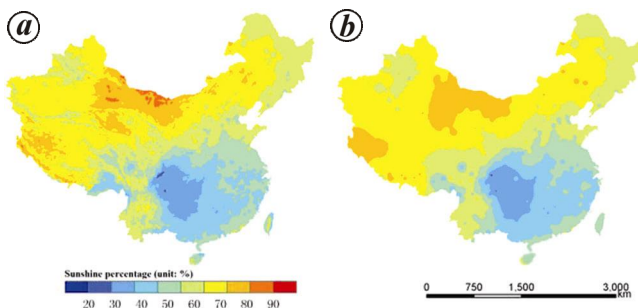**Figure 2.** Flow chart illustrating the procedure for calculating the sunshine duration.

Figure 3. Distribution of the annual mean sunshine percentage in 2001 determined using (*a*) model simulation and (*b*) interpolation of weather station observations.
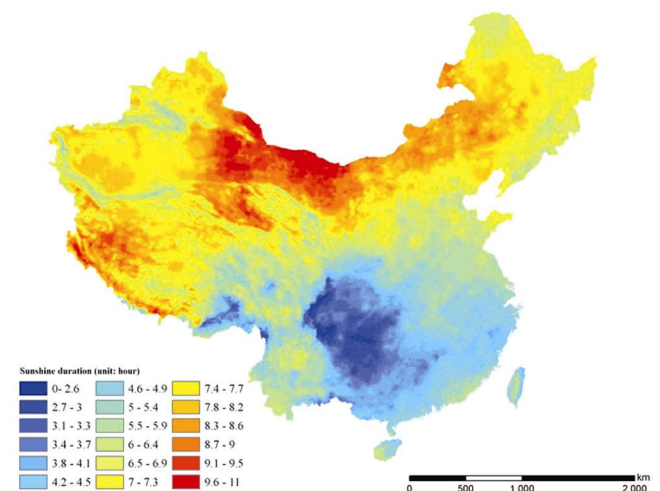

Figure 4. Distribution of the annual mean total daily sunshine duration in China in 2001.

Table 1. Difference between model and observed values of sunshine duration (SSD)

Month		January	February	March	April	May	June	July	August	September	October	November	December	Mean
Difference between model and standard weather station values of SSD														
2001	MABE (h)	0.21	0.18	0.26	0.18	0.17	0.15	0.18	0.15	0.16	0.16	0.23	0.22	0.19
	RABE (%)	4.29	3.39	3.93	2.98	2.55	2.49	2.49	2.45	2.95	2.88	3.79	4.43	3.22
2002	MABE (h)	0.22	0.19	0.23	0.18	0.16	0.15	0.16	0.16	0.17	0.18	0.22	0.2	0.19
	RABE (%)	4.3	3.36	3.91	2.89	2.56	2.34	2.55	2.45	2.72	2.88	3.88	4.64	3.21
2003	MABE (h)	0.23	0.18	0.22	0.18	0.17	0.15	0.17	0.16	0.17	0.18	0.22	0.24	0.19
	RABE (%)	4.17	3.26	3.88	2.93	2.68	2.52	2.65	2.58	2.86	3.05	4.01	4.53	3.26

Difference between model and intensive weather station values of SSD

	Jiangsu		Qinghai	
	Annual mean MABE (h)	Annual mean RABE (%)	Annual mean MABE (h)	Annual mean RABE (%)
2001	0.25	4.49	0.37	4.38
2002	0.25	4.33	0.32	4.32
2003	0.25	4.58	0.29	4.06

MABE, Mean absolute bias error; RABE, Relative bias error.

mean of MABE is approximately 0.3 h, and the annual mean of RABE is below 5%. Thus, the SSD model clearly has a strong modelling capability with respect to the spatial dimensions. Thus, the SSD model provides concrete, reliable results.

In conclusion, the major factors that influence the spatial and temporal distribution of SSD include the horizon screening (primarily rugged terrain) and atmospheric effects (primarily the cloud fraction). In the present study, we have developed a SSD model by taking into account these two factors and obtained spatial modelling of the actual SSD in China. The results of this study are summarized as follows:

(1) The SSD model developed here has a definitive physical meaning. Unlike the direct interpolation and terrain correction methods used in previous studies, this model characterizes the non-uniformity of the ground and atmosphere using DEM and remote sensing data to significantly improve the physical accuracy.

(2) The remote sensing data are incorporated into the SSD model, which takes full advantage of the contiguous satellite observations from space. The model reveals the patterns in the macroscopic SSD distribution in China. The regional SSD characteristics are clearly demonstrated by introducing DEM data, which fully account for the influence of terrain factors such as inclination and slope.

(3) The validation results for the calculation errors indicate that the as-developed SSD distribution model is reliable and stable. The MABE of the mean annual daily SSD is below 0.5 h, and the mean RABE is below 5%.

The principal goals of constructing a modern, publicly available meteorological service in China are to improve the coverage of weather information by acquiring environmental information at any time, on any spatial scale, and to expand the coverage of meteorological services. This study provides a basis for the spatialization of other meteorological data.

1. Angell, J. K., Variation in United States cloudiness and sunshine duration between 1950 and the drought year of 1988. *J. Climate*, 1990, **3**, 296–308.
2. Monteith, J. L., Climate and the efficiency of crop production in Britain. *Philos. Trans. R. Soc., London Ser. B*, 1977, **281**, 277–294.
3. Murray, S. J., Watson, I. M. and Prentice, I. C., The use of dynamic global vegetation models for simulating hydrology and the potential integration of satellite observations. *Prog. Phys. Geogr.*, 2012; doi: 10.1177/0309133312460072.
4. Weng, D. M., *Studies on Radiation Climate of Beijing* (in Chinese), *China*, China Meteorological Press, 1997.
5. Almorox, J. and Hontoria, C., Global solar radiation estimation using sunshine duration in Spain. *Energy Convers Manage.*, 2004, **45**, 1529–1535.
6. Ertekin, C. and Evrendilek, F., Spatio-temporal modeling of global solar radiation dynamics as a function of sunshine duration for Turkey. *Agric. For. Meteorol.*, 2007, **145**, 36–47.
7. Lam, J. C., Wan, K. K. W., Lau, C. C. S. and Yang, L., Climatic influences on solar modelling in China. *Renew. Energy*, 2008, **33**, 1591–1604.
8. Tang, W. J., Yang, K., He, J. and Qin, J., Quality control and estimation of global solar radiation in China. *Sol. Energy*, 2010, **84**, 466–475.
9. Tang, W. J., Yang, K., Qin, J. and Min, M., Development of a 50-year daily surface solar radiation dataset over China. *Sci. China Earth Sci.*, 2013; doi: 10.1007/s11430-012-4542-9.
10. Moradi, I., Quality control of global solar radiation using sunshine duration hours. *Energy*, 2009, **34**, 1–6.
11. Kothe, S., Good, E., Obregón, A., Ahrens, B. and Nitsche, H., Satellite-based sunshine duration for Europe. *Remote Sensing*, 2013, **5**, 2943–2972.
12. Wang, Y., Vertical distribution of sunshine duration in mountainous areas of Yunnan Province (in Chinese). *J. Mt. Sci.*, 1993, **11**, 1–8.
13. Ma, Z. F. and Tan, F., A study of the sunshine duration distribution trend and its application in the Tarim Basin (in Chinese). *Resour. Sci.*, 2000, **22**(2), 40–44.
14. Fu, B. P., Effects of sloping fields on sunshine and solar radiation (in Chinese). *J. Nanjing Univ.* (*Nat. Sci. Edn.*), 1958, **2**, 23–46.
15. Zhu, Z. H., The global distribution of astronomical solar radiation on nonhorizontal surfaces. *Sci. China* (*Ser. B*), 1988, **10**, 1100–1110.

16. Dolinar, M., Spatial interpolation of sunshine duration in Slovenia. *Meteorol. Appl.*, 2006, **13**(4), 375–384.
17. Hogewind, F. and Bissolli, P., Operational maps of monthly mean temperature for WMO Region VI (Europe and Middle East). *Idojaras*, 2011, **115**(1/2), 31–49.
18. Weng, D. M. and Luo, Z. X., *Mountainous Terrain Climate*, Meteorological Press, Beijing, 1990.
19. Zeng, Y., Qiu, X. F., Miao, Q. L. and Liu, C. M., Distribution of possible sunshine durations over rugged terrains of China. *Prog. Nat. Sci.*, 2003, **13**(10), 761–764.
20. Ding, S. G. *et al.*, Analysis of global variation in total cloud quantity over the past 20 years (in Chinese). *J. Appl. Meteorol. Sci.*, 2005, **16**, 670–678.
21. Renka, R. J., Multivariate interpolation of large sets of scattered data. *ACM Trans. Math. Software*, 1988, **14**(2), 139–148.
22. Liu, R. X. *et al.*, Analysis and validation of total cloud quantity data in China (in Chinese). *J. Appl. Meteorol. Sci.*, 2009, **20**, 571–578.
23. Cao, Y. *et al.*, Correction methods of MODIS cloud product based on ground observation data (in Chinese). *J. Remote Sensing*, 2012, **16**(2), 325–342.

Is Ganga the longest river in the Ganga Basin, India?

Neelam Verma, Rahul Devrani and Vimal Singh*

Department of Geology, Centre for Advanced Studies,
Chhatra Marg, University of Delhi, Delhi 110 007, India

The length of the main trunk in a river basin is an important morphometric parameter and it depends on the size of the drainage basin. The Ganga River Basin is one of the largest basins in the world with the Ganga River considered to be the main stem. Variable lengths of this river in the literature motivated us to study its exact length and also to test whether geomorphically it is the longest river in the basin. The results show that the maximum river length of 2758 km is attained when source is considered at the headstream of the Tons River. This length is more than any of the traditional lengths of the Ganga River in the literature. We propose to call the longest segment of the river in Ganga Basin as the Himalayan Foreland River.

Keywords: Ganga Basin, drainage network, headwater, river length, source stream.

*For correspondence. (e-mail: vimalgeo@gmail.com)

LARGE river systems have complex drainage network relationship in the hinterland. The Ganga River is one such system that includes several tributaries originating in the Himalaya, viz. Bhagirathi, Alaknanda, Yamuna, Ramganga, Ghaghara, Gandak and Kosi. Traditionally and culturally it is believed that the Ganga River originates from the Gangotri Glacier (Gaumukh). This point of origin has been used for the purpose of calculating the length of the river – that is often considered to be ~2600 km – based on which it is ranked 34th globally[1]. According to the United States of Geological Survey (USGS), 'a river's length may be considered to the distance from the mouth to the most distant headwater source (irrespective of stream name), or from the mouth to the headwaters of the stream commonly identified as the source stream'[2]. Therefore, exact length of a river can be determined by the position of its headwater (irrespective of whether it is perennial or ephemeral) and its embouchure (mouth)[3,4]. Farthest upstream point in a drainage network is defined as a source[5–7].

The Ganga River Basin comprises about 26.2% of the total land mass of India[8]. The Ganga River which originates in the Himalaya and flows through the Himalayan foreland is recognized as one of the main rivers in the Indian subcontinent. The name 'Ganga' is used after the Bhagirathi River joins the Alaknanda River at Devprayag. In the Ganga Basin, the axial river has more than one headwater and so it is difficult to define the source. Moreover, after the Farakka barrage, the river bifurcates into distributaries giving rise to different routes to the embouchure. This makes it difficult to extract the actual length of the Ganga River[9]. In the literature, the length of the Ganga River varies from slightly over 2500 km (refs 10 and 11) to 2650 km (ref. 8). In these studies, the source of the river is assumed to be at Gaumukh, and mouth of the river at the outfall of the Meghna River (also known as Lower Meghna) into the Bay of Bengal[8,10,11]. Parua[8] specified two different lengths for the Ganga considering different mouths of the river. According to him[8], the total length of the Ganga River from its origin at Gaumukh to its outfall to the sea via Hooghly and Meghna's course is 2645 km and 2650 km respectively.

Another important parameter of a river is its discharge and some workers believe that the stream that carries the largest volume of water should be the main stem[4]. The